Optimizing Power-frequency Droop Characteristics of Distributed Energy Resources

Swaroop S. Guggilam, *Student Member, IEEE*, Changhong Zhao, *Member, IEEE*, Emiliano Dall'Anese, *Member, IEEE*, Yu Christine Chen, *Member, IEEE*, and Sairaj V. Dhople, *Member, IEEE*

***Abstract*—This paper outlines a procedure to design power-frequency droop slopes for distributed energy resources (DERs) installed in distribution networks to optimally participate in primary frequency response. In particular, the droop slopes are engineered such that DERs respond in proportion to their power ratings and they are not unfairly penalized in power provisioning based on their location in the distribution network. The main contribution of our approach is that a guaranteed level of frequency regulation can be guaranteed at the feeder head, while ensuring that the outputs of individual DERs conform to some well-defined notion of fairness. The approach we adopt leverages an optimization-based perspective and suitable linearizations of the power-flow equations to embed notions of fairness and information regarding the physics of the power flows within the distribution network into the droop slopes. Time-domain simulations from a differential algebraic equation model of the 39-bus New England test-case system augmented with three instances of the IEEE 37-node distribution-network with frequency-sensitive DERs are provided to validate our approach.**

***Index Terms*—Distributed energy resources, droop control, primary frequency response.**

NOMENCLATURE

P_k, Q_k	net non-frequency-sensitive active- and reactive-power injections at bus k
P_{kj}, Q_{kj}	active and reactive power flows on branch (k, j)
$\|V_k\|\angle\theta_k$	Voltage phasor at bus k
y_{kj}	series admittance of transmission line (k, j)
y_{kj}^{sh}	shunt admittance on both ends of transmission line (k, j)
ω_{s}	synchronous frequency
$\Delta\omega$	frequency offset from the synchronous frequency
ΔP_k	change in the real power injections at bus k from equilibrium value
ΔP_{kj}	change in active-power flow on branch (k, j) from equilibrium value
D_g	load-damping coefficient at generator bus g
$R_{\mathcal{G},g}$	frequency-power speed-droop regulation constant of generator g
D_ℓ^f	droop coefficient of DER ℓ in feeder f
$R_{\mathcal{F},f}^{-1}$	frequency regulation provided by DERs in feeder f
R_{eff}^{-1}	network-wide frequency regulation characteristic

S. S. Guggilam and S. V. Dhople are with the Department of Electrical and Computer Engineering, University of Minnesota, Minneapolis, MN 55455, USA. E-mail: {guggi022, sdhople}@umn.edu. C. Zhao and E. Dall'Anese are with the National Renewable Energy Laboratory, Golden, CO. E-mail: {changhong.zhao, emiliano.dallanese}@nrel.gov. Y. C. Chen is with the Department of Electrical and Computer Engineering, The University of British Columbia, Vancouver, British Columbia V6T 1Z4. E-mail: chen@ece.ubc.ca

The effort of S. S. Guggilam, C. Zhao, E. Dall'Anese, and S. V. Dhople was primarily supported by the Advanced Research Projects Agency-Energy (ARPA-E) under the Network Optimized Distributed Energy Systems (NODES) program. S. S. Guggilam, S. V. Dhople were also supported in part by the National Science Foundation (NSF) through grant CyberSEES 1442686 and CAREER award ECCS-1453921.

I. INTRODUCTION

APPROACHES for regulating system frequency in power transmission systems are based on inertial response, primary frequency response, and automatic generation control. This work focuses on primary frequency response, which is traditionally achieved exclusively via governor control from a subset of synchronous generators in the system. To supplement governor control, this paper outlines a method to optimize the participation of distributed energy resources (DERs) in primary-frequency response recognizing their growing penetration in power distribution networks. The proposed design process achieves two overarching objectives. The droop coefficients for individual DERs are designed so that: i) in aggregate, a distribution network with a collection of frequency-responsive DERs offers a guaranteed power-frequency-droop characteristic at the transmission-distribution interface—a notion that we refer to as *inter-feeder regulation*, and ii) the DER power outputs can be engineered to be proportional to their ratings and compensate for their location on the distribution feeder—in essence, we can ensure *intra-feeder fairness*. By meeting these two objectives, transmission *and* distribution networks are collectively acknowledged, and DERs are ensured to participate optimally in primary-frequency response. The focus of this effort is at the transmission-distribution interface, an important area of research that is recently receiving attention in the literature. It is worth mentioning that there is a wide body of work on the tangentially related problem of DER dispatch focused on improving power quality within distribution networks (see, e.g., [1]–[3] and pertinent references therein).

Figure 1 exemplifies the vision of the proposed approach. The objective is to design synthetic frequency-droop coefficients, D_ℓ^f, for DERs located in feeder f, so that the active power injected at the feeder head, P_f^{in}, is modulated in response to frequency deviations $\Delta\omega_f$ via the power-frequency droop relationship $\Delta\omega_f = R_{\mathcal{F},f}\Delta P_f^{\text{in}}$, where $R_{\mathcal{F},f}$ is the system-operator-specified regulation constant. Furthermore,

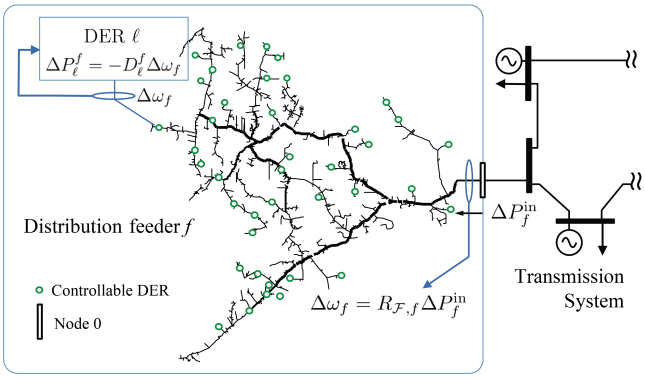

Fig. 1. The proposed approach demonstrates how power-frequency droop slopes for individual DERs, D_ℓ^f, can be designed so that: i) the f distribution feeder presents a frequency-regulation characteristic, $R_{\mathcal{F},f}$, at the feeder head, and ii) the injections of individual DERs, ΔP_ℓ^f, conform to a well-defined notion of fairness.

the individual-DER power outputs, i.e., $\Delta P_\ell^f = -D_\ell^f \Delta\omega_f$ should be regulated following some notion of fairness. As an example, one option would be to ensure that the DERs respond in proportion to their power ratings. In particular, the ratio $\Delta P_\ell^f / \overline{P}_\ell^f$ ($\overline{P}_\ell^f$ denotes the rated power of DER ℓ in feeder f) should be the same for all the DERs. The procedure we outline to design power-frequency droop characteristics leverages: i) suitable linear approximations of the AC power-flow equations [4], [5]; and ii) an optimization-based perspective that ensures fairness of participation and adherence to pertinent electrical laws and limits. Consequently, the droop coefficients embed information regarding: the locations of the DERs, their power ratings, power flows within the network, and the prescribed regulation at the feederhead. It is obvious that business-as-usual approaches, e.g., suppose all DERs are naively regulated to provide 5% regulation, would not yield guaranteed regulation $R_{\mathcal{F},f}$ at the feeder head. Within this context, the procedure outlined in this work is fair—in the sense that DERs participate based on their power ratings, and ensures the desired regulation—in the sense that the system operator has a guarantee on the frequency regulation on offer from an aggregation of DERs.

Calling upon DERs to participate in ancillary services such as primary-frequency control requires them to potentially ramp up and ramp down their output power in response to a frequency event. This has monetary implications [6], particularly when renewable-based DERs have to curtail power [7], [8]. It also assumes that DERs such as PV and wind energy conversion systems have the ability to potentially operate away from the maximum power point to ensure the possibility of dispatching up or down [9]–[11]. Depending on prevailing ambient conditions, DERs may need to be augmented with storage to ensure primary-frequency response capability.

Recognizing the growing importance of DERs in power distribution networks, several efforts have investigated how these could complement traditional generation-side capabilities by providing ancillary services at multiple time scales focusing on frequency regulation [12]–[14]. Given the focus of our work, we next overview pertinent literature that has dwelt on: how controllers can be designed so that DERs can participate in primary-frequency response, and how optimization can be leveraged as a tool for engineering primary-frequency response capability of DERs. For instance, [11], [15]–[22] focus on DER-level controller design for inertial and primary-frequency control from DERs such as wind and photovoltaic energy conversion systems. Similarly, [23]–[25] investigate load-side participation for primary frequency response. The scope of these efforts is restricted to the transmission network, i.e., details of power flows within the distribution feeder are ignored for simplicity. On a related note, an optimization-based approach to engineer damping constants and synthetic inertia constants is provided in [26]. This method is tailored to transient dynamics since it is based on explicitly computing the system eigenvalues. A unit commitment method targeting frequency-response specifications with a particular focus on wind energy systems using battery energy storage was developed in [27].

This work offers some fundamental contributions over prior art pertaining to DER participation in frequency control. Primarily, we acknowledge the physics of the power flows within the distribution network in engineering primary-frequency-response capability. In particular, this means that the DERs are not penalized for their location on the distribution feeder when contributing to primary-frequency response. Furthermore, while previous approaches offer limited guarantees on the power outputs of individual DERs, we incorporate fairness principles in the design of the droop slopes so that DERs are not unfairly penalized in terms of how much power they are called upon to provide for primary-frequency response based on their capacity or location on the feeder. To summarize, the ability to guarantee a prescribed level of frequency regulation at the feeder head, while congruently ensuring equitable participation of DERs in primary frequency response, is the main contribution of this work over approaches discussed previously.

A preliminary version of our efforts appears in [28]. Here, we expand on this by: i) formalizing optimization problems to justify and guide the design of the droop coefficients while embedding desired fairness notions in the cost functions, ii) demonstrating design strategies for the case when the DERs do not have the same power ratings, and iii) validating the approach with time-domain simulations in a large power-system dynamic model. In particular, a 39-bus New England test-case system is considered, and augmented with three instances of a 37-node distribution-network with frequency-sensitive DERs to illustrate the approach.

The remainder of this paper is organized as follows. In Section II, the notation adopted in the paper and the system model are described. Power-flow equations and dynamical models adopted for the generators and DERs are spelled out in Section III. The optimization-based formulation to engineer droop slopes for fairness and frequency regulation is presented in Section IV. The proposed design method is validated in Section V with a suite of numerical simulations. Finally, concluding remarks and directions for future work are highlighted in Section VI.

II. Preliminaries

In this section, we first establish notation and then describe the power-system model.

A. Notation

The matrix inverse is denoted by $(\cdot)^{-1}$, transpose by $(\cdot)^{\mathrm{T}}$, complex conjugate by $(\cdot)^*$, real and imaginary parts of a complex number by $\mathrm{Re}\{\cdot\}$ and $\mathrm{Im}\{\cdot\}$, respectively, and $\mathrm{j} := \sqrt{-1}$. A diagonal matrix formed with diagonal entries composed of entries of vector x is denoted by $\mathrm{diag}(x)$. For a matrix X, X_{mn} returns the entry in the m row and n column of X and $X_{n,\cdot}$ denotes nth row of X.

B. Network Model

Next, we introduce the notation used to describe the transmission and distribution networks.

1) Transmission Network: We consider a classical power-network model for the transmission grid, which is represented by a graph, where $\mathcal{N} := \{1, \ldots, |\mathcal{N}|\}$ is the set of buses, and $\mathcal{E} \subset \mathcal{N} \times \mathcal{N}$ is the set of transmission lines. A transmission line is denoted by $(g, \ell) \in \mathcal{E}$. We denote by $\mathcal{G} \subset \mathcal{N}$, the set of buses that are connected to conventional turbine-based generators.

2) Distribution Network: Denote, by $\mathcal{F} \subset \mathcal{N}$, the set of buses in the transmission system where distribution feeders are present. Node 0 denotes the secondary side of the distribution substation transformer. Accordingly, nodes of the distribution feeder connected to transmission system bus $f \in \mathcal{F}$, are collected in the set $\mathcal{B}_f \cup \{0\}$, $\mathcal{B}_f := \{1, \ldots, |\mathcal{B}_f|\}$. Furthermore, for the distribution feeder connected to transmission system bus $f \in \mathcal{F}$, let $\mathcal{D}_f \subseteq \mathcal{B}_f$ (with cardinality $|\mathcal{D}_f|$) denote the set of nodes where frequency-sensitive DERs are present. For the subsequent discussions, we consider only one feeder per bus $f \in \mathcal{F}$. This can readily be generalized at the risk of complicating notation.

III. System Model and Problem Statement

In this section, we discuss the power-flow model, pertinent dynamical models for synchronous generators and DERs, and steady-state frequency regulation.

A. Power-flow Model

Transmission line (k, j) is modeled using the lumped-element π-model with series admittance $y_{kj} = y_{jk} = g_{kj} + \mathrm{j}b_{kj} \in \mathbb{C}\backslash\{0\}$ and shunt admittance $y_{kj}^{\mathrm{sh}} = g_{kj}^{\mathrm{sh}} + \mathrm{j}b_{kj}^{\mathrm{sh}} \in \mathbb{C}\backslash\{0\}$ on both ends of the line. The power injections at buses $k \in \mathcal{N} \cup (\cup_{f\in\mathcal{F}}\mathcal{B}_f)$ are given by

$$0 = P_k - \sum_{j\in\mathcal{N}_k} P_{kj}, \qquad 0 = Q_k - \sum_{j\in\mathcal{N}_k} Q_{kj}, \tag{1}$$

where $\mathcal{N}_k$ is the set of buses electrically connected to bus k, and P_k and Q_k are the net non-frequency-sensitive active- and reactive-power injections at bus k. Following standard power-flow computations, the branch flows P_{kj}, Q_{kj}, are given by

$$\begin{aligned} P_{kj} &= |V_k|^2(g_{kj}^{\mathrm{sh}} + g_{kj}) \\ &\quad - |V_k||V_j|\left(g_{kj}\cos\theta_{kj} + b_{kj}\sin\theta_{kj}\right) \\ Q_{kj} &= -|V_k|^2(b_{kj}^{\mathrm{sh}} + b_{kj}) \\ &\quad - |V_k||V_j|\left(g_{kj}\sin\theta_{kj} - b_{kj}\cos\theta_{kj}\right), \end{aligned} \tag{2}$$

where the voltage phasor at bus k is given by $|V_k|\angle\theta_k$ and $\theta_{kj} := \theta_k - \theta_j$.

B. System Dynamical Models

We describe the dynamical model for the generators in the transmission network, and then discuss the frequency-responsive DER model.

1) Transmission Network: We model the dynamics of angular position, frequency, and mechanical-power input for the generators in the network since we are interested in time scales in the regime of primary frequency response. Particularly, for the $g \in \mathcal{G}$ generator, we adopt the following third-order dynamical model:

$$\begin{aligned} \dot{\theta}_g &= \omega_g - \omega_{\mathrm{s}} \\ M_g\dot{\omega}_g &= P_g^{\mathrm{m}} - D_g(\omega_g - \omega_{\mathrm{s}}) + P_g - \sum_{k\in\mathcal{N}_g} P_{gk} \\ \tau_g\dot{P}_g^{\mathrm{m}} &= -P_g^{\mathrm{m}} + P_g^{\mathrm{r}} - \frac{1}{R_{\mathcal{G},g}}(\omega_g - \omega_{\mathrm{s}}). \end{aligned} \tag{3}$$

Above, θ_g, ω_g, and P_g^{m} are the dynamical states for rotor electrical angular position, generator frequency, and turbine mechanical power, respectively, for the gth generator, and ω_{s} is the synchronous frequency. Also, M_g is the inertia constant, D_g is the load-damping coefficient, $R_{\mathcal{G},g}$ is the frequency-power speed-droop regulation constant, τ_g is the turbine time constant, and P_g^{r} denotes its reference power setting. Since we do not model dynamics pertinent to secondary control, we assume P_g^{r} to be a constant. Finally, P_g is the injection at bus g, and P_{gk} is the real-power flow from bus g to k. This is a negative quantity if it corresponds to a constant-power load. Since we are concerned with time scales pertaining to primary frequency response, we disregard the automatic voltage regulator and exciter dynamics, and assume that the excitation voltage is constant in the model.

2) Distribution Network: Assume the following model for the power-electronics-based zero-inertia DERs connected to nodes $\ell \in \mathcal{D}_f$ in feeder $f \in \mathcal{F}$

$$\begin{aligned} \dot{\theta}_\ell &= \omega_f - \omega_{\mathrm{s}}, \\ 0 &= P_\ell - \sum_{j\in\mathcal{N}_\ell} P_{\ell j} - D_\ell^f(\omega_f - \omega_{\mathrm{s}}), \end{aligned} \tag{4}$$

where $P_{\ell j}$ is active power flow in branch (ℓ, j). The above model is appropriate for DERs in a setting where the frequency at the feeder head (connected to the transmission network) percolates down to all nodes in the feeder [23]. The droop coefficient $D_\ell^f > 0$ establishes the frequency response of the DER at node ℓ. Next, we analyze the steady-state frequency offset that results from the dynamics (1)–(4). The above model is only appropriate for time scales pertaining to primary

frequency response. The dynamics at faster time scales for different DERs would indeed vary based on the type of DER and inner-loop controllers employed.

C. Steady-state Frequency Regulation

Given the combined transmission and distribution system model in (1)–(4), we quantify the steady-state frequency offset that results from a power imbalance in the network and the equivalent regulation constant combining all the feeders in the network. Assume the system initially operates at the synchronous steady-state equilibrium point. Then, suppose an imbalance in active-power generation and consumption arises in the network. In particular, we define the disturbance

$$\begin{aligned}\Delta P_{\text{dist}} := &\sum_{g\in\mathcal{G}}(\Delta P_g - \sum_{\ell\in\mathcal{N}_g}\Delta P_{g\ell})\\ &+ \sum_{f\in\mathcal{B}_f}(\Delta P_f - \sum_{\ell\in\mathcal{N}_f}\Delta P_{f\ell}),\end{aligned} \tag{5}$$

where $\Delta P_g, \Delta P_f, \Delta P_{g\ell}$, and $\Delta P_{f\ell}$ denote changes in the real-power nodal and line injections from their equilibrium values in (3) and (4). Since we are interested in a time horizon where secondary control has not yet acted (i.e., P_g^{r} remains constant), we note that the post-disturbance steady-state frequency does not correspond to the synchronous frequency. Let us define $\Delta\omega$ to be the frequency offset from the synchronous frequency. Summing up all nodal real-power balance equations (including instances of (3) $\forall\, g \in \mathcal{G}$ and (4) $\forall\, \ell \in \mathcal{D}_f, f \in \mathcal{F}$) at the new steady-state operating point, and solving for $\Delta\omega$

$$\Delta\omega = \frac{\Delta P_{\text{dist}}}{\sum_{g\in\mathcal{G}}(R_{\mathcal{G},g}^{-1} + D_g) + \sum_{f\in\mathcal{F}}\sum_{\ell\in\mathcal{D}_f} D_\ell^f} =: \frac{\Delta P_{\text{dist}}}{R_{\text{eff}}^{-1}}. \tag{6}$$

Given an operator-prescribed network-wide frequency regulation characteristic, R_{eff}^{-1}, (typically specified in units of $[\text{MW}/0.1\text{Hz}]$ [29]), the goal is to design the D_ℓ^f's such that

$$\sum_{f\in\mathcal{F}}\sum_{\ell\in\mathcal{D}_f} D_\ell^f =: \sum_{f\in\mathcal{F}} R_{\mathcal{F},f}^{-1} = R_{\text{eff}}^{-1} - \sum_{g\in\mathcal{G}}(R_{\mathcal{G},g}^{-1} + D_g), \tag{7}$$

where $R_{\mathcal{F},f}^{-1}$ corresponds to the frequency regulation provided by feeder $f \in \mathcal{F}$.

The expression in (6) relates the steady-state frequency offset to the *net* power imbalance. Given the developments leading up to this model, this model is valid for disturbances that are step changes, fast ramps, etc. For other disturbances types that evolve as more general functions of time, one would need to consider detailed generator dynamics and possibly the dynamics of DER controllers in the analysis. Performance specifications that go beyond steady-state frequency regulation would presumably be important in such settings.

D. Problem Statement

With the definition of the per-feeder frequency-regulation characteristic, $R_{\mathcal{F},f}^{-1}$, in (7), the design problem is to determine $\{D_\ell^f\}_{f\in\mathcal{F},\ell\in\mathcal{D}_f}$ to achieve two overarching objectives:

- *Inter-feeder regulation*: The frequency response of the DERs is such that, in aggregate, the distribution feeder presents a frequency-regulation characteristic, $R_{\mathcal{F},f}^{-1}$, at the feeder head.
- *Intra-feeder fairness*: The power outputs of the DERs for primary-frequency response, i.e., $\Delta P_\ell^f = -D_\ell^f \Delta\omega_f$ correspond to some notion of fairness that captures, e.g., the DER power ratings and ensures that the DERs are not penalized in terms of power provisioning based on their location in the feeder.

At the outset, it is not clear how to achieve either objective mentioned above. Particularly, there are infinite options for the individual D_ℓ^f's that satisfy (7). Additionally, we have—as of yet—not quantified any notion of optimality to guide the selection of the D_ℓ^f's. We address both concerns by systematically formulating and outlining solutions to feeder-level optimization problems next. To simplify notation, we drop the superscript f when referring to the droop slopes. In particular, D_ℓ subsequently denotes the droop slope for the ℓ-th DER in the f feeder.

The scope of the problem we address does not include how the system operator would specify the network-wide frequency regulation characteristic, R_{eff}^{-1}, or the values of the individual feeder-level frequency regulation constants, $R_{\mathcal{F},f}^{-1}$. We assume these are known constants in our problem formulation. A variety of considerations pertaining to power quality, economics, and the nature of the distribution network (in terms of the types, capacities, and numbers of DERs installed) could factor into the choice of $R_{\mathcal{F},f}^{-1}$ and R_{eff}^{-1}.

IV. Engineering Droop Coefficients

An optimization-based perspective is adopted to design the D_ℓ's to satisfy the two objectives outlined in Section III-D. First, we formulate an economic-dispatch-type problem that determines the optimal pre-disturbance operating point for the DERs, and thereafter, we outline an auxiliary problem defined around the pre-disturbance optimal operating point with the droop slopes serving as decision variables. We illustrate how different notions of intra-feeder fairness can be translated to synthesize appropriate cost functions, and in each case, ensure desired frequency regulation by incorporating it as a constraint. It should be clear that these optimization problems are solely intended to justify the design process for the D_ℓ's and they are not advocated for outlining real-time operational strategies.

A. Optimal Dispatch Problem

At the transmission level, the system operator runs economic dispatch, e.g., every 5 minutes, to determine the reference power injections P_g^{r} for generators $g \in \mathcal{G}$ and the reference power flows $P_f^{\text{in,r}}$ into feeder $f \in \mathcal{F}$. Analogously, one can envision the following optimal DER dispatch problem for feeder $f \in \mathcal{F}$:

$$\min_{P_\ell^{\text{r}},\, \ell\in\mathcal{D}_f} \quad \sum_{\ell\in\mathcal{D}_f} c_\ell(P_\ell^{\text{r}}) \tag{8a}$$

$$\text{s.t.} \quad P_f^{\text{in,r}} = \sum_{\ell\in\mathcal{B}_f} \varphi_\ell P_\ell^{\text{r}} + c_{p,f}, \tag{8b}$$

where $\varphi \in \mathbb{R}^{1\times|\mathcal{B}_f|}$ can be interpreted as participation factor that map the contribution of active power injections to the

real-power flow at the feeder head, and $c_{\mathrm{p},f} \in \mathbb{R}$ is a network topology dependent constant. Equation (8b) follows from a linearization of the power-flow equations (see Appendix A for details), and $P_f^{\mathrm{in,r}}$ is an input to the problem specified by the system operator. In (8), decision variables include only DER active-power output P_ℓ^{r} for $\ell \in \mathcal{D}_f$. However, we can easily extend the problem to include reactive-power output as decision variables (in the case where DERs participate in reactive-power support), voltage limits, and capacity constraints [5]. A key question of course, is how to pick the cost functions, c_ℓ, since the DERs are largely expected to have zero marginal cost of operation [30]. Furthermore, notice that the problem in (8) is only defined at the pre-disturbance steady state, and as such the droop slopes do not appear in the formulation. Nonetheless it provides a rigorous starting point for our design approach. As discussed subsequently, this will be based on formulating an auxiliary optimization problem defined around the optimizers of (8), with the droop slopes serving as decision variables.

B. Auxiliary Optimization Problem and Closed-form Solution

We formulate the following optimization problem to design droop coefficients D_ℓ for DERs $\ell \in \mathcal{D}_f$, such that a target droop coefficient $R_{\mathcal{F},f}$ is achieved for the power flow P_f^{in} down the head of feeder f, with minimum cost at the post-disturbance steady state. We consider steady-state operation, and treat $\Delta\omega$ as a disturbance in the analysis. This leads to the following formulation:

$$\min_{D_\ell, \ell \in \mathcal{D}_f} \quad \sum_{\ell \in \mathcal{D}_f} c_\ell(P_\ell^{\mathrm{r},\star} - D_\ell \Delta\omega) \tag{9a}$$

$$\text{s.t.} \quad \frac{1}{R_{\mathcal{F},f}} \Delta\omega = \sum_{\ell \in \mathcal{D}_f} \varphi_\ell \left(-D_\ell \Delta\omega\right), \tag{9b}$$

where $\{P_\ell^{\mathrm{r},\star}\}_{\ell \in \mathcal{D}_f}$ are the optimizers of (8), and the DER droop slopes D_ℓ are the decision variables. Next, we obtain the closed-form solution to (9) by assuming small perturbations around the optimizer of (8). We assume that the cost function $c_\ell(\cdot), \forall\, \ell \in \cup_{f \in \mathcal{F}} \mathcal{D}_f$ is *strictly convex* and *twice continuously differentiable*.

Consider the DER dispatch problem in (8). Let $\{P_\ell^{\mathrm{r},\star}\}_{\ell \in \mathcal{D}_f}$ be the optimizers of (8). Let λ^{r} denote the dual variable, i.e., the Lagrangian multiplier for the constraint (8b). By the Karush-Kuhn-Tucker (KKT) conditions [31, Section 5.5.3], and strict convexity of the objective (8a), problem (8) has a unique pair of optimizers $(\{P_\ell^{\mathrm{r},\star}\}_{\ell \in \mathcal{D}_f}, \lambda^{\mathrm{r},\star})$ which satisfy

$$c_\ell'(P_\ell^{\mathrm{r},\star}) := \left.\frac{dc_\ell}{dP_\ell^{\mathrm{r}}}\right|_{P_\ell^{\mathrm{r},\star}} = \lambda^{\mathrm{r},\star} \varphi_\ell. \tag{10}$$

Next, consider the problem in (9) as a perturbation on the solution of (8) and define the following auxiliary cost function:

$$\widetilde{c}_\ell(D_\ell) := c_\ell(P_\ell^{\mathrm{r},\star} - D_\ell \Delta\omega). \tag{11}$$

For the same reason as that for (10), (9) has a unique pair of optimizers $(\{D_\ell^\star\}_{\ell \in \mathcal{D}_f}, \lambda^\star)$ which satisfy

$$\left.\frac{d\widetilde{c}_\ell}{dD_\ell}\right|_{D_\ell^\star} = -c_\ell'(P_\ell^{\mathrm{r},\star} - D_\ell^\star \Delta\omega)\Delta\omega = -\lambda^\star \varphi_\ell \Delta\omega, \tag{12}$$

where $\lambda^\star$ is the value of Lagrangian multiplier for the constraint in (9b) at the optimal solution. Since we consider small perturbations around the optimizers of (8), we will find it convenient for subsequent analysis to define

$$\Delta\lambda^\star = \lambda^\star - \lambda^{\mathrm{r},\star}. \tag{13}$$

Since $\Delta\omega \neq 0$, we can drop it from both sides of (12). Considering $-D_\ell^\star \Delta\omega$ as a small perturbation on $P_\ell^{\mathrm{r},\star}$, we expand $c_\ell'(P_\ell^{\mathrm{r},\star} - D_\ell^\star \Delta\omega)$ in a first-order Taylor series around $P_\ell^{\mathrm{r},\star}$ as

$$\begin{aligned} c_\ell'(P_\ell^{\mathrm{r},\star} - D_\ell^\star \Delta\omega) &\approx c_\ell'(P_\ell^{\mathrm{r},\star}) - c_\ell''(P_\ell^{\mathrm{r},\star}) D_\ell^\star \Delta\omega \\ &= (\lambda^{\mathrm{r},\star} + \Delta\lambda^\star)\varphi_\ell. \end{aligned} \tag{14}$$

The second equality follows from substituting for $\lambda^\star$ from (13) in the right-hand side of (12). Isolating $D_\ell^\star$ while recognizing that $c_\ell'(P_\ell^{\mathrm{r},\star}) = \lambda^{\mathrm{r},\star}\varphi_\ell$ (see (10)), we arrive at:

$$D_\ell^\star = -\frac{\Delta\lambda^\star}{\Delta\omega} \cdot \frac{\varphi_\ell}{c_\ell''(P_\ell^{\mathrm{r},\star})}. \tag{15}$$

Note that by our assumptions on $c_\ell(\cdot)$, the functions $c_\ell'(\cdot)$ and $c_\ell''(\cdot)$ exist, and $c_\ell''(\cdot)$ is strictly positive.

The structure of optimal $D_\ell^\star$ in (15) implies that $\forall\, k, \ell \in \mathcal{D}_f$

$$\frac{\varphi_k D_k^\star}{\varphi_\ell D_\ell^\star} = \left(\frac{\varphi_k^2}{c_k''(P_k^{\mathrm{r},\star})}\right)\left(\frac{\varphi_\ell^2}{c_\ell''(P_\ell^{\mathrm{r},\star})}\right)^{-1}. \tag{16}$$

Congruently, constraint (9b) requires

$$\sum_{k \in \mathcal{D}_f} \varphi_k D_k^\star = -\frac{1}{R_{\mathcal{F},f}}. \tag{17}$$

From (16) and (17) we have

$$\varphi_\ell D_\ell^\star = -\frac{1}{R_{\mathcal{F},f}} \frac{\varphi_\ell^2}{c_\ell''(P_\ell^{\mathrm{r},\star})} \left(\sum_{k \in \mathcal{D}_f} \frac{\varphi_k^2}{c_k''(P_k^{\mathrm{r},\star})}\right)^{-1},$$

and therefore

$$D_\ell^\star = -\frac{1}{R_{\mathcal{F},f}} \frac{\varphi_\ell}{c_\ell''(P_\ell^{\mathrm{r},\star})} \left(\sum_{k \in \mathcal{D}_f} \frac{\varphi_k^2}{c_k''(P_k^{\mathrm{r},\star})}\right)^{-1}. \tag{18}$$

Before proceeding, we bring to attention two important points. First, while the frequency offset $\Delta\omega$ appeared as an external disturbance in the problem formulation (9), the expressions for the droop slopes in (18) only depends on the individual DER characteristics, the desired feeder-level frequency-regulation specification, and the network. Also, we note that the optimization setup in (8) that was used as a foundation in the analysis is only valid in integrated power systems where system operators may run economic dispatch. In settings where schedules are formulated based on the outcome of energy transactions, one could conceptualize the quantities $\lambda^\star$ and $P_\ell^\star$ (leveraged in and following (9)) to be the price of traded power in the transaction and the transacted power, respectively.

C. Notions of Fairness

The power injected by DER ℓ for primary frequency response, $\Delta P_\ell = -D_\ell^\star \Delta\omega$, where $D_\ell^\star$ is obtained from the solution to (9). Next, we show that different modes of DER participation in frequency regulation can be enforced by appropriately defining cost functions $\{c_\ell(P_\ell^{\mathrm{r}})\}_{\ell\in\mathcal{D}_f}$ in (8). Particularly, we describe three settings in decreasing order of how fairly the DERs participate in steady-state frequency droop response, quantified by the values of ΔP_ℓ in each case. We will find that ensuring greater fairness of participation requires more information to be shared across DERs in the network.

1) Contributions proportional to capacities: Suppose the power injections of DERs $\ell \in \mathcal{D}_f$ can only change in the range $\Delta P_\ell \in \big[-\overline{P}_\ell, \overline{P}_\ell\big]$, where the control capacity $\overline{P}_\ell$ depends not only on the power rating of DER ℓ but also its reference power injection $P_\ell^{\mathrm{r},\star}$. We are interested in the setting where the power injections of the DERs are in proportion to their power ratings:

$$\frac{\Delta P_1}{\overline{P}_1} = \frac{\Delta P_2}{\overline{P}_2} = \cdots = \frac{\Delta P_{|\mathcal{D}_f|}}{\overline{P}_{|\mathcal{D}_f|}}. \tag{19}$$

Based on this, the DER droop slopes must satisfy, $\forall\, k, \ell \in \mathcal{D}_f$,

$$\frac{D_k^\star \Delta\omega}{\overline{P}_k} = \frac{D_\ell^\star \Delta\omega}{\overline{P}_\ell} \implies \frac{\varphi_k}{\overline{P}_k c_k''(P_k^{\mathrm{r},\star})} = \frac{\varphi_\ell}{\overline{P}_\ell c_\ell''(P_\ell^{\mathrm{r},\star})},$$

where the implication results by substituting (18). Therefore, the power-injections in (19) can be guaranteed by solving (9) with cost functions that satisfy

$$c_\ell''(P_\ell^{\mathrm{r},\star}) = \rho \frac{\varphi_\ell}{\overline{P}_\ell},$$

where $\rho > 0$ is some constant. An example of such a cost function, and resulting optimal droop slope are

$$c_\ell(P_\ell) = \frac{1}{2}\frac{\varphi_\ell}{\overline{P}_\ell} P_\ell^2,\ D_\ell = -R_{\mathcal{F},f}^{-1}\overline{P}_\ell\Big(\sum_{k\in\mathcal{D}_f}\varphi_k \overline{P}_k\Big)^{-1}. \tag{20}$$

2) Equal contributions: Suppose we wish to engineer the droop slopes so that the change in power outputs of all the DERs for primary frequency response are the same. Particularly, we desire

$$\Delta P_1 = \Delta P_2 = \cdots = \Delta P_{|\mathcal{D}_f|}. \tag{21}$$

Based on this, the DER droop slopes must satisfy, $\forall\, k, \ell \in \mathcal{D}_f$,

$$D_k^\star \Delta\omega = D_\ell^\star \Delta\omega \implies \frac{\varphi_k}{c_k''(P_k^{\mathrm{r},\star})} = \frac{\varphi_\ell}{c_\ell''(P_\ell^{\mathrm{r},\star})},$$

where the implication results by substituting (18). Therefore, the power-injections in (21) can be guaranteed by solving (9) with cost functions that satisfy

$$c_\ell''(P_\ell^{\mathrm{r},\star}) = \rho\varphi_\ell,$$

where $\rho > 0$ is some constant. An example of such a cost function, and resulting optimal droop slope are

$$c_\ell(P_\ell) = \frac{1}{2}\varphi_\ell P_\ell^2, \quad D_\ell = -R_{\mathcal{F},f}^{-1}\Big(\sum_{k\in\mathcal{D}_f}\varphi_k\Big)^{-1}. \tag{22}$$

3) Equal Contributions at Feeder Head: Finally, consider the setting where we require the effective contributions of the DERs measured at the feeder head to be the same. Particularly, we require

$$\varphi_1 \Delta P_1 = \varphi_2 \Delta P_2 = \cdots = \varphi_{|\mathcal{D}_f|}\Delta P_{|\mathcal{D}_f|}. \tag{23}$$

Based on this, the DER droop slopes must satisfy, $\forall\, k, \ell \in \mathcal{D}_f$,

$$\varphi_k D_k^\star \Delta\omega = \varphi_\ell D_\ell^\star \Delta\omega \implies \frac{\varphi_k^2}{c_k''(P_k^{\mathrm{r},\star})} = \frac{\varphi_\ell^2}{c_\ell''(P_\ell^{\mathrm{r},\star})},$$

where, as before, the implication results by substituting (18). Therefore, the power injections in (19) can be guaranteed by solving (9) with cost functions that satisfy

$$c_\ell''(P_\ell^{\mathrm{r},\star}) = \rho\varphi_\ell^2,$$

where $\rho > 0$ is some constant. An example of such a cost function, and resulting optimal droop slope are

$$c_\ell(P_\ell) = \frac{1}{2}\varphi_\ell^2 P_\ell^2, \quad D_\ell = -R_{\mathcal{F},f}^{-1}\varphi_\ell^{-1}|\mathcal{D}_f|^{-1}. \tag{24}$$

Having outlined the three modes of DER participation above, we offer the following comments on how fair the three options are, and how much information is needed to realize each option:

- Of the three options, the one in (19) is the most fair, since DERs participate in proportion to their power ratings. Contrast this with the case (23). The values of φ_ℓ tend to reduce as we move away from the feeder head (we do not have an analytical justification for this, but we observe this numerically [28]). Therefore, even though (23) ensures that the effective contributions of DERs are equal at the feederhead, DERs located further from the feederhead contribute more power. This is seen in our simulation results (see Fig. 6(c′)).
- Of the three options, the one in (19) requires most information to be shared across DERs. In particular, the optimal value of D_ℓ (20) depends on all the φ_ℓ's and $\overline{P}_\ell$'s. Contrast this with the choice of D_ℓ in (24) which does not depend on any information about other DERs in the network.

V. Case Studies

We simulate the 10-machine New-England power system, where $\mathcal{N} = \{1, 2, 3, \ldots, 39\}$, with generators connected at buses in $\mathcal{G} = \{1, 2, \ldots, 10\}$ [32], [33]. In addition, we augment this system with three identical 37-node distribution feeders equipped with frequency-responsive DERs, with the feeder heads connected to buses in $\mathcal{F} = \{10, 12, 14\}$, as shown in Fig. 2. Each identical instantiation of the distribution feeder contains frequency-responsive DERs, $\mathrm{D1}, \ldots, \mathrm{D9}$, at nodes $\mathcal{D}_f = \{1, 4, 7, 11, 12, 14, 19, 22, 33\}$, $\forall\, f \in \mathcal{F}$, as shown in Fig. 3. The 37-node distribution feeder used is a suitably modified version of the IEEE 37-node distribution test feeder [34]. Pertinent network and model parameters are listed in Appendix B. For convenience, voltage magnitudes are in per unit [pu] with a 4.8 [kV] base, and power and impedance

values are also in [pu] with base 1000 [MVA], unless otherwise specified. Ensuing results are obtained from time-domain simulations of the combined transmission-distribution-network model, performed with the Power System Toolbox (PST) [35]. The machine model considered in PST is more realistic and detailed in comparison to the analytical model in (3); particularly, the PST model includes a detailed two-axis subtransient reactance generator model, and a DC12 exciter model for terminal-voltage regulation.

In our time-domain simulations, at time $t = 0\,[\text{sec}]$, the load at bus 18 in the transmission network undergoes a step increase of $\Delta P_{18} = 0.3$. We investigate primary frequency response for this setting in the following cases:

(i) Only the generators in the transmission network provide primary frequency response. None of the DERs are frequency sensitive, i.e., $D_\ell^f = 0, \forall \ell \in \cup_{f\in\mathcal{F}}\mathcal{D}_f$. As a protective measure, DERs cease injecting real power when the system frequency drops below 59.75 [Hz] [36].

(ii) Only the generators in the transmission network provide primary frequency response. However, under frequency load shedding capability of 0.02 [pu] is available when system frequency drops below 59.75 [Hz] [37].

(iii) Case (i), except, DERs across all three 37-node distribution feeder collected in the set $\mathcal{D}_{10}$, $\mathcal{D}_{12}$, and $\mathcal{D}_{14}$ also contribute to primary frequency response. Droop slopes for individual DERs are selected to satisfy the criterion in (19).

(iv) Same setting as Case (iii), except, the droop slopes for individual DERs are selected according to the criterion in (21).

(v) Same setting as Case (iii), except, the droop slopes for individual DERs are selected according to the criterion in (23).

Note that steady-state frequency regulation of $14.6[\text{MW}/0.1\text{Hz}]$ is selected as the operator's choice, and in response to that we needed total regulation $\sum R_{\mathcal{F},f}^{-1} = 33$ using (6). The prescribed frequency-regulation constants at the feeder head in each case are set to be $R_{\mathcal{F},10}^{-1} = 11, R_{\mathcal{F},12}^{-1} = 10, R_{\mathcal{F},14}^{-1} = 12$. Since we assume that all the feeders are identical, we distribute $\sum R_{\mathcal{F},f}^{-1}$ regulation approximately equally to each feeder.

We first comment on the improvement in steady-state frequency regulation afforded by the DERs, then on the effect of penetration of DERs on system frequency response, and finally, we dwell on the power outputs of the DERs for cases (iii)–(v).

A. Steady-state Frequency Regulation

Figure 4 shows the evolution of frequency at bus 10 (as a particular instance) in the transmission network for case (i) (only generators provide frequency support), case (ii) (in addition to generator frequency support, system frequency is controlled with under frequency load shedding), and case (v) (in addition to generator frequency support, frequency-sensitive DERs provide primary frequency support with droop slopes selected according to (24)). The system frequency response under cases (iii) and (iv) are similar to that in (v) (since in

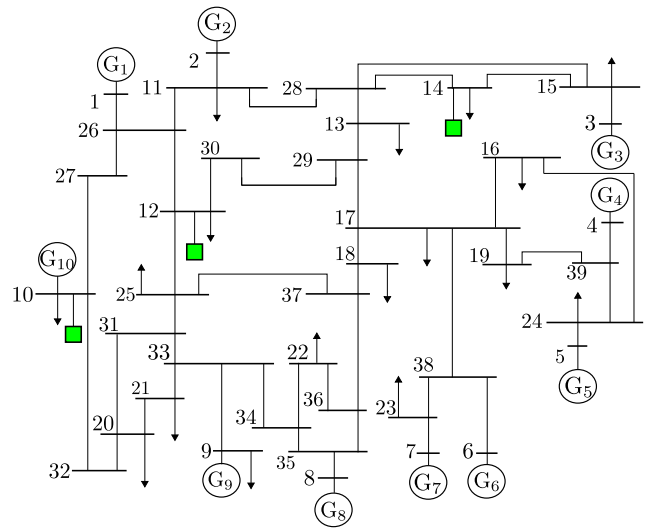

Fig. 2. Power network used in the case study is composed of the New England 39-bus system, and three instances of a modified IEEE 37-node test feeder connected to buses $\mathcal{F} = \{10, 12, 14\}$ in the transmission system (illustrated as green squares).

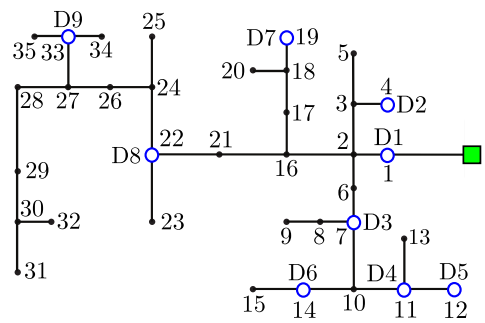

Fig. 3. Modified IEEE 37-node distribution test feeder model. The model includes nine frequency-responsive DERs, $\text{D}1, \ldots, \text{D}9$. Three instances of this feeder are connected to buses $\mathcal{F} = \{10, 12, 14\}$ in the transmission system in Fig. 2 (illustrated as green squares).

cases (iii)-(v), the DERs cumulatively yield the same feeder-level regulation), and these cases are not plotted. In case (i), there is additional loss of generation 0.25 [pu] since the system frequency drops below 59.71 [Hz], at which point the DERs cease injecting real power. From (6), we expect that

$$\Delta\omega = \frac{\Delta P_{\text{dist}}}{\sum_{g\in\mathcal{G}}(D_g + R_{\mathcal{G},g}^{-1})} = 0.0048,$$

which corresponds to a steady-state frequency of 59.71 [Hz]. In the above equation, $\Delta P_{\text{dist}} = \Delta P_{18} + 0.25 = 0.55$ [pu] (i.e., it includes the original disturbance and the subsequent loss of DER generation). In case (ii), in addition to the generator frequency support, we have load shedding of 0.02 [pu] and from (6) we expect that

$$\Delta\omega = \frac{\Delta P_{\text{dist}}}{\sum_{g\in\mathcal{G}}(D_g + R_{\mathcal{G},g}^{-1})} = 0.0025,$$

which corresponds to a steady-state frequency of 59.85 [Hz]. In the above equation, $\Delta P_{\text{dist}} = \Delta P_{18} - 0.02 = 0.28$ [pu] (i.e., it includes the original disturbance and the subsequent load

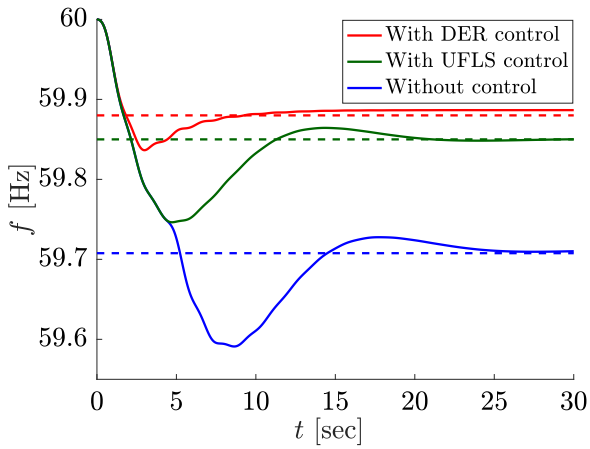

Fig. 4. Frequency at bus 10 after the load step at bus 18. The steady-state frequency offset with frequency-sensitive DERs is significantly lower. Steady-state results from time-domain simulations (solid lines) match the analytical results (dashed lines).

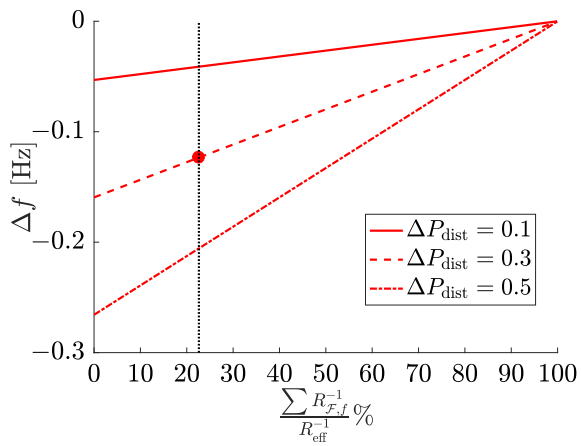

Fig. 5. Steady-state frequency offset as a function of DER penetration level (fraction of the total frequency regulation in the system contributed to by DERs) for different load steps. The red circle corresponds to the simulation setting in cases (iii)-(v).

shedding). Finally, in case (v), where the DERs also contribute to frequency regulation, the cut-off value is not reached and, we expect from (6) that

$$\Delta\omega = \frac{\Delta P_{18}}{\sum\limits_{g\in\mathcal{G}}(D_g + R_{\mathcal{G},g}^{-1}) + \sum\limits_{f\in\mathcal{F}}\sum\limits_{\ell\in\mathcal{D}_f} D_\ell^f} = 0.0020,$$

which corresponds to a steady-state frequency of 59.88 [Hz]. In each case, the steady-state values predicted above are plotted as dashed lines in Fig. 4, and they are seen to correspond to the values that result from the detailed time-domain simulation.

The results in Fig. 4 confirm that controlling the DERs improves steady-state performance compared to the case where only the generators provide frequency response. Furthermore, the match in steady-state between the time-domain simulation results (in solid lines) and the analytical results (dashed lines) validates the assumptions and analyses leading up to (6). The small error in steady state value is because the expression for ΔP_{dist} in (6) includes the losses, which is not modeled above.

B. Effect of Penetration of DERs

In Section V-A, we showed how DERs improve the system frequency response with a particular load disturbance. Here, we investigate how system frequency responds under different load disturbances as a function of DER penetration. Figure 5 depicts the steady-state frequency offset as a function of DER penetration level—quantified here in terms of the fraction of the total frequency regulation in the system contributed to by DERs—for different load steps. Our simulation setup represents a penetration level of 23% , and the expected frequency offset for different disturbances are obtained as intersections of the vertical dashed line (black) with the the red curves. The red dot indicates the operating point for the test case analyzed in previous Section V-A, i.e., the red curve in Fig. 4.

C. Power Outputs of DERs

We now comment on the power outputs of the DERs for cases (ii), (iii) and (iv) and corresponding notions of fairness. In all cases, we illustrate results for the distribution feeder installed at bus 14 without loss of generality.

(ii) The cost functions are selected as in (20). Capacities for the DERs are defined as $2\overline{P}_1 = 2\overline{P}_2 = 2\overline{P}_3 = 2\overline{P}_4 = 2\overline{P}_5 = \overline{P}_6 = \overline{P}_7 = \overline{P}_8 = \overline{P}_9$. In Fig. 6(a), we plot $\Delta P_\ell/\Delta P_{\text{dist}}$ through the load step. Notice that the DERs respond in proportion to their ratings as desired. In particular, DERs $6, 7, 8, 9$ provide twice as much power as DERs $1, 2, 3, 4, 5$.

(iii) By selecting cost functions as in (22), we can ensure that all DERs contribute equal amounts of active power toward primary frequency response. We plot the quantities $\Delta P_\ell/\Delta P_{\text{dist}}$ in Fig. 6(b) and it can indeed be seen that each DER injects the same active power. This could be construed to be unfair given the ratings of the DERs mentioned previously.

(iv) By selecting cost functions as in (24), we can ensure that DERs provide the same effective power at the feeder head. In Fig. 6(c), we plot $|\varphi_\ell \Delta P_\ell/\Delta P_{\text{dist}}|$ through the load step, and it can indeed be seen that the effective power provided by each DER at the feeder head is the same, i.e., $\varphi_k \Delta P_k = \varphi_l \Delta P_l, \forall\, k, l \in \mathcal{D}_f$. However, in this setting, the ones farther away from the feeder head contribute more active power while providing primary frequency support. In order to see this effect, we plot the normalized quantity $(\Delta P_\ell - \Delta P_1)100/\Delta P_{\text{dist}}$ in Fig. 6(c′), where ΔP_1 is the change in active-power injection at the DER closest to the feeder head.

In steady state, the sum of the changes in real-power injections of all DERs installed on the feeder located at bus 14 are equal to 0.273, 0.264, and 0.271 in cases (iii), (iv), and (v), respectively. The corresponding changes in real-power injections at the feeder head are 0.208, 0.209, and 0.207. As expected, these numbers confirm that the same effective frequency-regulation

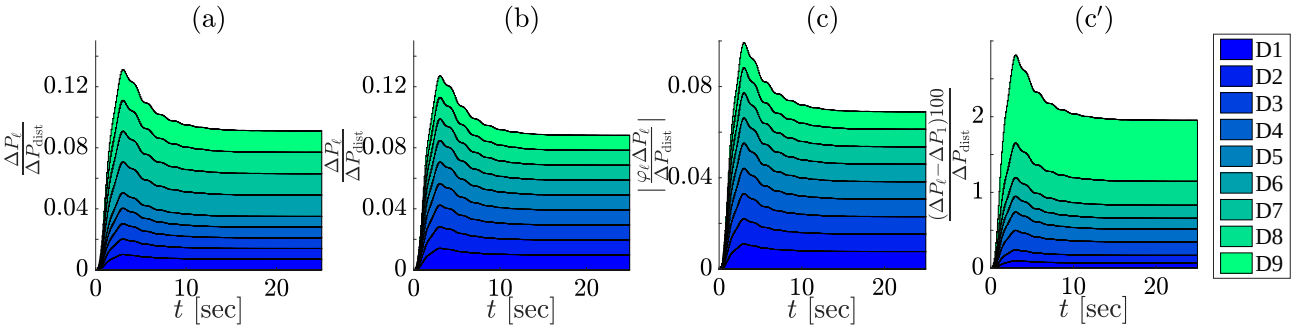

Fig. 6. (a) Droop slopes are engineered such that DERs provide injections proportional to their capacities. (b) Droop slopes are engineered such that each DER provides equal power. (c) Droop slopes are engineered such that DERs provide the same effective contributions at the feeder head. (c′) Relative contributions of each DER (with respect to the one installed closest to the feeder head) indicate how a naïve choice of droop coefficients in (c) penalizes the ones that are far from the feeder head.

is provided at the feeder head even though the individual DER power injections are different. (Numbers for the other two feeders are similar, and not reported for conciseness.)

VI. Concluding Remarks and Directions for Future Work

In this paper, we proposed a method to design power-frequency droop characteristics for individual DERs in a distribution feeder so that, in aggregate, they provide a prescribed primary frequency response at the feeder head. The method leverages linear approximations of the AC power-flow equations to embed participation factors into the design of the droop slopes such that the change in injections from the DERs can be engineered to follow different notions of fairness.

Developing multi phase models for the proposed control scheme, designing systematic methods for rigorous stability and convergence analyses are compelling avenues for future work. Also, while the purpose of formulating the optimization problems in (8)–(9) was to obtain a rigorous solution procedure for the droop slopes, systematic integration of similar problems with bulk-system economic dispatch is a compelling direction for future work. Finally, while we focus on primary-frequency control, if DERs are endowed with synthetic inertia, then they can also be called upon for inertial control. One would then need to uncover the mapping between time-domain performance specifications like the frequency nadir and rate of change of frequency to the DER damping and inertia terms. This is part of our ongoing investigations.

Appendix

A. Approximation of Power Flowing into Distribution Feeder

Let $V_n \in \mathbb{C}$ and $I_n \in \mathbb{C}$ denote the phasors for the line-to-ground voltage at and the current injected into node n, respectively, and define the $|\mathcal{B}_f|$-dimensional complex vectors $V := [V_1, \ldots, V_{|\mathcal{B}_f|}]^{\mathrm{T}} \in \mathbb{C}^{|\mathcal{B}_f|}$ and $I := [I_1, \ldots, I_{|\mathcal{B}_f|}]^{\mathrm{T}} \in \mathbb{C}^{|\mathcal{B}_f|}$. Also, let V_0 denote the voltage at the secondary side of the distribution transformer, and let I_0 denote the current injected into the distribution feeder $f \in \mathcal{F}$. We can write

$$\begin{bmatrix} I_0 \\ I \end{bmatrix} = \begin{bmatrix} y_{00} & \bar{y}^{\mathrm{T}} \\ \bar{y} & Y \end{bmatrix} \begin{bmatrix} V_0 \\ V \end{bmatrix} =: Y_{\mathrm{net}} \begin{bmatrix} V_0 \\ V \end{bmatrix}, \qquad (25)$$

where the system admittance matrix $Y_{\mathrm{net}} \in \mathbb{C}^{|\mathcal{B}_f|+1 \times |\mathcal{B}_f|+1}$ is partitioned in sub-matrices with the following dimensions: $Y \in \mathbb{C}^{|\mathcal{B}_f| \times |\mathcal{B}_f|}$, $\bar{y} \in \mathbb{C}^{|\mathcal{B}_f| \times 1}$, and $y_{00} \in \mathbb{C}$. Linearizing the power-flow equations, the following relationship between the power at the feeder head $S_f^{\mathrm{in}} = P_f^{\mathrm{in}} + \mathrm{j}Q_f^{\mathrm{in}}$ and the nodal power injections $P, Q \in \mathbb{R}^{|\mathcal{B}_f|}$ throughout the feeder can be established [28]:

$$\begin{bmatrix} P_f^{\mathrm{in}} \\ Q_f^{\mathrm{in}} \end{bmatrix} = \begin{bmatrix} \varphi \\ \zeta \end{bmatrix} P + \begin{bmatrix} \alpha \\ \beta \end{bmatrix} Q + \begin{bmatrix} c_{\mathrm{p},f} \\ c_{\mathrm{q},f} \end{bmatrix} \qquad (26)$$

where $\varphi \in \mathbb{R}^{1 \times |\mathcal{B}_f|}$, $\zeta \in \mathbb{R}^{1 \times |\mathcal{B}_f|}$, $\alpha \in \mathbb{R}^{1 \times |\mathcal{B}_f|}$, $\beta \in \mathbb{R}^{1 \times |\mathcal{B}_f|}$, $c_{\mathrm{p},f} \in \mathbb{R}$ and $c_{\mathrm{q},f} \in \mathbb{R}$ are given by

$$\begin{bmatrix} \varphi \\ \zeta \\ \alpha \\ \beta \end{bmatrix} = \begin{bmatrix} -\psi_1 & 0 & \psi_2 & 0 \\ \psi_2 & 0 & \psi_1 & 0 \\ 0 & -\psi_1 & 0 & \psi_2 \\ 0 & \psi_2 & 0 & \psi_1 \end{bmatrix} \begin{bmatrix} H_{1,\cdot}^{11} \\ H_{1,\cdot}^{12} \\ H_{1,\cdot}^{21} \\ H_{1,\cdot}^{22} \end{bmatrix} \qquad (27)$$

$$\begin{bmatrix} c_{\mathrm{p},f} \\ c_{\mathrm{q},f} \end{bmatrix} = |V_0|^2 \begin{bmatrix} 1 & 1 & 0 & 0 \\ 0 & 0 & -1 & -1 \end{bmatrix} \begin{bmatrix} g_{01}, g_0, b_{01}, b_0 \end{bmatrix}^{\mathrm{T}}$$
$$+ \begin{bmatrix} -\psi_1 & \psi_2 & -\psi_1 & \psi_2 \\ \psi_2 & \psi_1 & \psi_2 & \psi_1 \end{bmatrix} \begin{bmatrix} \mathrm{Re}\{V_{\mathrm{nom},1}\} \\ \mathrm{Im}\{V_{\mathrm{nom},1}\} \\ -H_{1,\cdot}^{11} P_{\mathrm{nom}} - H_{1,\cdot}^{12} Q_{\mathrm{nom}} \\ -H_{1,\cdot}^{21} P_{\mathrm{nom}} - H_{1,\cdot}^{22} Q_{\mathrm{nom}} \end{bmatrix}.$$

Above, the following parameters were defined for conciseness:

$$\psi_1 = |V_0|(\cos(\theta_0) g_{01} + \sin(\theta_0) b_{01})$$
$$\psi_2 = |V_0|(\cos(\theta_0) b_{01} - \sin(\theta_0) g_{01})$$
$$H = \begin{bmatrix} \mathrm{Re}\{\Gamma\} + \mathrm{Re}\{\Xi\} & -\mathrm{Im}\{\Gamma\} + \mathrm{Im}\{\Xi\} \\ \mathrm{Im}\{\Gamma\} + \mathrm{Im}\{\Xi\} & \mathrm{Re}\{\Gamma\} - \mathrm{Re}\{\Xi\} \end{bmatrix}^{-1}$$
$$\Gamma = \mathrm{diag}\left(Y^* V_{\mathrm{nom}}^* + \bar{y}^* V_0^*\right), \quad \Xi = \mathrm{diag}\left(V_{\mathrm{nom}}\right) Y^*,$$

where V_{nom} is the linearization point. In typical distribution networks, entries of α are much smaller than those of φ (we observe this empirically [28]); this implies that reactive-power injections minimally impact the active-power flow on the feeder head. Therefore, the real-power flow on the feeder head can be approximated as $P_f^{\mathrm{in}} \approx \sum_{\ell \in \mathcal{B}_f} \varphi_\ell P_\ell + c_{\mathrm{p},f}$; this appears in the constraint of (8b). Furthermore, when there is a perturbation around the nominal injection, we get

$\Delta P_f^{\text{in}} \approx \sum_{\ell \in \mathcal{B}_f} \varphi_\ell \Delta P_\ell$, and this expression is leveraged in constraint (9b).

B. Simulation parameters

The synchronous frequency, $\omega_{\text{s}} = 2\pi 60\,[\text{rad}\,\text{sec}^{-1}]$. All values are reported in per unit unless otherwise noted.

Parameters of Transmission System: The network topology and power injections are in accordance to the standard IEEE New-England power system. We modify a few parameters for our simulations. Generator damping coefficients are: $D_1 = ... = D_{10} = 2$, droop coefficients are: $R_{\mathcal{G},1}^{-1} = 3.7, R_{\mathcal{G},2}^{-1} = 8.6, R_{\mathcal{G},3}^{-1} = 9.7, R_{\mathcal{G},4}^{-1} = 9.5, R_{\mathcal{G},5}^{-1} = 7.6, R_{\mathcal{G},6}^{-1} = 9.7, R_{\mathcal{G},7}^{-1} = 8.4, R_{\mathcal{G},8}^{-1} = 8.1, R_{\mathcal{G},9}^{-1} = 12.4, R_{\mathcal{G},10}^{-1} = 15$, turbine time constants are $\tau_1 = ... = \tau_{10} = 5\,[\text{sec}]$.

Parameters of Distribution System: The network topology and power injections are in accordance to the standard IEEE 37-node test feeder [34]. While this is a three-phase feeder, we assume balanced operation, and use data from phase 2 for our simulation. We add $y_{kk}^{\text{sh}} = 0.004 + \text{i}0.005, \forall\, k \in \{2, \ldots, 18\} \subset \mathcal{B}_3$ and $y_{kk}^{\text{sh}} = 0.006 + \text{i}0.007, \forall\, k \in \{18, \ldots, 35\} \subset \mathcal{B}_3$. The base voltage is $4.8\,[\text{kV}]$.

References

[1] K. Turitsyn, P. Sulc, S. Backhaus, and M. Chertkov, "Options for control of reactive power by distributed photovoltaic generators," *Proceedings of the IEEE*, vol. 99, no. 6, pp. 1063–1073, June 2011.

[2] V. Calderaro, V. Galdi, F. Lamberti, and A. Piccolo, "A smart strategy for voltage control ancillary service in distribution networks," *IEEE Transactions on Power Systems*, vol. 30, no. 1, pp. 494–502, Jan 2015.

[3] S. Soltani, M. Rashidinejad, and A. Abdollahi, "Stochastic multiobjective distribution systems phase balancing considering distributed energy resources," *IEEE Systems Journal*, 2017, to be published.

[4] S. V. Dhople, S. S. Guggilam, and Y. C. Chen, "Linear approximations to AC power flow in rectangular coordinates," in *53rd Annual Allerton Conference on Communication, Control, and Computing*, 2015, pp. 211–217.

[5] S. S. Guggilam, E. Dall'Anese, Y. C. Chen, S. V. Dhople, and G. B. Giannakis, "Scalable optimization methods for distribution networks with high PV integration," *IEEE Transactions on Smart Grid*, vol. 7, no. 4, pp. 2061–2070, Jul 2016.

[6] C. Y. Tee and J. B. Cardell, "Market integration of distributed resources through coordinated frequency and price droop," *IEEE Transactions on Smart Grid*, vol. 5, no. 4, pp. 1556–1565, 2014.

[7] A. N. M. M. Haque, M. T. Rahman, P. H. Nguyen, and F. W. Bliek, "Smart curtailment for congestion management in LV distribution network," in *2016 IEEE Power and Energy Society General Meeting*, July 2016, pp. 1–5.

[8] C. Shao, X. Wang, M. Shahidehpour, X. Wang, and B. Wang, "Security-constrained unit commitment with flexible uncertainty set for variable wind power," *IEEE Transactions on Sustainable Energy*, vol. 8, no. 3, pp. 1237–1246, July 2017.

[9] W. Liu, X. Liu, Z. Jiang, N. Li, and D. Xi, "Overview of advanced control technology for wind power generation," in *2016 IEEE 11th Conference on Industrial Electronics and Applications (ICIEA)*, June 2016, pp. 706–711.

[10] J. Seuss, M. J. Reno, M. Lave, R. J. Broderick, and S. Grijalva, "Advanced inverter controls to dispatch distributed PV systems," in *2016 IEEE 43rd Photovoltaic Specialists Conference (PVSC)*, June 2016, pp. 1387–1392.

[11] V. Gevorgian and B. O'Neill, "Advanced grid-friendly controls demonstration project for utility-scale PV power plants," National Renewable Energy Laboratory, Golden, CO, USA, Tech. Rep., 2016.

[12] J. A. Short, D. G. Infield, and L. L. Freris, "Stabilization of grid frequency through dynamic demand control," *IEEE Transactions on Power Systems*, vol. 22, no. 3, pp. 1284–1293, Jul 2007.

[13] A. Molina-Garcia, F. Bouffard, and D. S. Kirschen, "Decentralized demand-side contribution to primary frequency control," *IEEE Transactions on Power Systems*, vol. 26, no. 1, pp. 411–419, Feb 2011.

[14] B. Xu, A. Oudalov, J. Poland, A. Ulbig, and G. Andersson, "BESS control strategies for participating in grid frequency regulation," *IFAC Proceedings Volumes*, vol. 47, no. 3, pp. 4024–4029, Aug 2014.

[15] V. A. K. Pappu, B. Chowdhury, and R. Bhatt, "Implementing frequency regulation capability in a solar photovoltaic power plant," in *Proceedings of North American Power Symposium*, Arlington, Texas, USA, 2010, pp. 1–6.

[16] V. Gevorgian, Y. Zhang, and E. Ela, "Investigating the impacts of wind generation participation in interconnection frequency response," *IEEE Transactions on Sustainable Energy*, vol. 6, no. 3, pp. 1004–1012, Jul 2015.

[17] S. Ghosh, S. Kamalasadan, N. Senroy, and J. Enslin, "Doubly Fed Induction Generator (DFIG)-Based Wind Farm Control Framework for Primary Frequency and Inertial Response Application," *IEEE Transactions on Power Systems*, vol. 31, no. 3, pp. 1861–1871, May 2016.

[18] J. V. de Vyver, J. D. M. D. Kooning, B. Meersman, L. Vandevelde, and T. L. Vandoorn, "Droop control as an alternative inertial response strategy for the synthetic inertia on wind turbines," *IEEE Transactions on Power Systems*, vol. 31, no. 2, pp. 1129–1138, March 2016.

[19] A. A. Thatte, F. Zhang, and L. Xie, "Coordination of wind farms and flywheels for energy balancing and frequency regulation," in *Power and Energy Society General Meeting, 2011 IEEE*. IEEE, 2011, pp. 1–7.

[20] J. W. Choi, S. Y. Heo, and M. K. Kim, "Hybrid operation strategy of wind energy storage system for power grid frequency regulation," *IET Generation, Transmission & Distribution*, vol. 10, no. 3, pp. 736–749, 2016.

[21] A. W. Korai and I. Erlich, "Frequency dependent voltage control by der units to improve power system frequency stability," in *Proceedings of IEEE Eindhoven PowerTech*, June 2015, pp. 1–6.

[22] A. Ghafouri, J. Milimonfared, and G. B. Gharehpetian, "Coordinated control of distributed energy resources and conventional power plants for frequency control of power systems," *IEEE Transactions on Smart Grid*, vol. 6, no. 1, pp. 104–114, 2015.

[23] M. Donnelly, D. Harvey, R. Munson, and D. Trudnowski, "Frequency and stability control using decentralized intelligent loads: Benefits and pitfalls," in *Proceedings of IEEE Power and Energy Society General Meeting*, Minneapolis, MN, USA, 2010, pp. 1–6.

[24] A. Kasis, E. Devane, C. Spanias, and I. Lestas, "Primary frequency regulation with load-side participation part I: stability and optimality," *IEEE Transactions on Power Systems*, 2017, to be published.

[25] E. Devane, A. Kasis, M. Antoniou, and I. Lestas, "Primary frequency regulation with load-side participation part II: beyond passivity approaches," *IEEE Transactions on Power Systems*, vol. PP, no. 99, pp. 1–1, 2017, to be published.

[26] T. S. Borsche, T. Liu, and D. J. Hill, "Effects of rotational inertia on power system damping and frequency transients," in *IEEE Conference on Decision and Control*, December 2015, pp. 5940–5946.

[27] Y. Wen, W. Li, G. Huang, and X. Liu, "Frequency dynamics constrained unit commitment with battery energy storage," *IEEE Transactions on Power Systems*, vol. 31, no. 6, pp. 5115–5125, 2016.

[28] S. S. Guggilam, C. Zhao, E. Dall'Anese, Y. C. Chen, and S. V. Dhople, "Primary frequency response with aggregated ders," in *2017 American Control Conference*, May 2017, pp. 3386–3393.

[29] A. Moeini and I. Kamwa, "Analytical concepts for reactive power based primary frequency control in power systems," *IEEE Transactions on Power Systems*, vol. 31, no. 6, pp. 4217–4230, November 2016.

[30] J. A. Taylor, S. V. Dhople, and D. S. Callaway, "Power systems without fuel," *Renewable and Sustainable Energy Reviews*, vol. 57, pp. 1322–1336, 2016.

[31] S. Boyd and L. Vandenberghe, *Convex Optimization*. Cambridge University Press, 2004.

[32] T. Athay, R. Podmore, and S. Virmani, "A practical method for the direct analysis of transient stability," *IEEE Transactions on Power Apparatus and Systems*, no. 2, pp. 573–584, 1979.

[33] M. A. Pai, *Energy function analysis for power system stability*. Springer Science & Business Media, 2012.

[34] (2016) IEEE Power and Energy Society distribution test feeders. [Online]. Available: https://ewh.ieee.org/soc/pes/dsacom/testfeeders/.

[35] J. Chow and G. Rogers, *Power System Toolbox*. Cherry Tree Scientific Software, 2000.

[36] T. S. Basso and R. DeBlasio, "IEEE 1547 series of standards: interconnection issues," *IEEE Transactions on Power Electronics*, vol. 19, no. 5, pp. 1159–1162, 2004.

[37] P. M. Anderson and M. Mirheydar, "An adaptive method for setting underfrequency load shedding relays," *IEEE Transactions on Power Systems*, vol. 7, no. 2, pp. 647–655, May 1992.

Swaroop S. Guggilam (S'15) received the Bachelor's degree in electrical engineering from the Veermata Jijabai Technological Institute, Mumbai, Maharashtra, India, in 2013 and M.S. degree in electrical engineering from the University of Minnesota, Minneapolis, MN, USA, in 2015. He is currently working toward the Ph.D. degree in electrical engineering from the University of Minnesota, Minneapolis, MN, USA.

His research interests include distribution networks, optimization, power system modeling, analysis and control for increasing renewable integration.

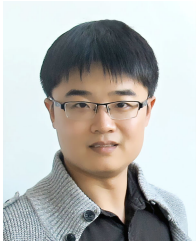

Changhong Zhao (S'12-M'15) received the B. Eng. degree in Automation from Tsinghua University in 2010, and the PhD degree in Electrical Engineering from California Institute of Technology in 2016. His PhD thesis won the Caltech Demetriades-Tsafka-Kokkalis Prize and the Caltech Charles Wilts Prize. He is currently a Research Engineer with National Renewable Energy Laboratory, Golden, CO, USA, with research interests in power system dynamics and stability, optimal power flow, distributed control of smart grid, and multi-energy systems.

Emiliano Dall'Anese (S'08-M'11) received the Laurea Triennale (B.Sc Degree) and the Laurea Specialistica (M.Sc Degree) in Telecommunications Engineering from the University of Padova, Italy, in 2005 and 2007, respectively, and the Ph.D. In Information Engineering from the Department of Information Engineering, University of Padova, Italy, in 2011. From January 2009 to September 2010, he was a visiting scholar at the Department of Electrical and Computer Engineering, University of Minnesota, USA. From January 2011 to November 2014 he was a Postdoctoral Associate at the Department of Electrical and Computer Engineering and Digital Technology Center of the University of Minnesota, USA. Since December 2014 he has been a Senior Engineer at the National Renewable Energy Laboratory, Golden, CO, USA.

His research interests lie in the areas of Optimization Theory and Signal Processing. Current applications pertain to distributed optimization and control of large-scale complex energy systems and power-grid analytics.

Yu Christine Chen (S'10–M'15) received the B.A.Sc. degree in engineering science from the University of Toronto, Toronto, ON, Canada, in 2009, and the M.S. and Ph.D. degrees in electrical engineering from the University of Illinois at Urbana-Champaign, Urbana, IL, USA, in 2011 and 2014, respectively.

She is currently an Assistant Professor with the Department of Electrical and Computer Engineering, The University of British Columbia, Vancouver, BC, Canada, where she is affiliated with the Electric Power and Energy Systems Group. Her research interests include power system analysis, monitoring, and control.

Sairaj V. Dhople (S'09-M'13) received the B.S., M.S., and Ph.D. degrees in electrical engineering, in 2007, 2009, and 2012, respectively, from the University of Illinois, Urbana-Champaign. He is currently an Assistant Professor in the Department of Electrical and Computer Engineering at the University of Minnesota (Minneapolis), where he is affiliated with the Power and Energy Systems research group. His research interests include modeling, analysis, and control of power electronics and power systems with a focus on renewable integration. Dr. Dhople received the National Science Foundation CAREER Award in 2015. He currently serves as an Associate Editor for the IEEE Transactions on Energy Conversion.